2008

Flicker Attenuation—Part I: Response of Three-Phase Induction Motors to Regular Voltage Fluctuations

S. Tennakoon
University of Wollongong

S. Perera
University of Wollongong, sarath@uow.edu.au

D. Robinson
Beca Pty. Ltd, Australia

Flicker Attenuation—Part I: Response of Three-Phase Induction Motors to Regular Voltage Fluctuations

Abstract

Voltage fluctuations leading to lamp flicker that originate in one place in a power system tend to propagate to other parts of the network with some level of attenuation depending on the network impedances and the loads connected. Numerous subsynchronous- type frequency components exist in these voltage fluctuations that are responsible for lamp flicker. The rudimentary theory and the experimental measurements support the idea that industrial load bases, which contain a large percentage of mains-connected induction motors, tend to attenuate flicker better compared to residential load bases having mainly passive loads. This paper reports on the response of three-phase induction motors of several sizes when subjected to low-frequency voltage fluctuations: 1) the case where a balanced single-frequency component is superimposed on the mains voltage and 2) the case where the mains voltage is sinusoidally amplitude modulated, a scheme that is frequently used in the flicker-related work. Small-signal models are presented that will enable systematic understanding of the behavior which is verified using large signal models.

Keywords

Flicker, flicker attenuation, induction motors, small-signal models.

Disciplines

Physical Sciences and Mathematics

Publication Details

This article was originally published as Tennakoon, S, Perera, S & Robinson, D, Flicker Attenuation—Part I: Response of Three-Phase Induction Motors to Regular Voltage Fluctuations, IEEE Transactions on Power Delivery, 23(2), 2008, 1207-1214.

Flicker Attenuation—Part I: Response of Three-Phase Induction Motors to Regular Voltage Fluctuations

S. Tennakoon, *Student Member, IEEE*, S. Perera, *Member, IEEE*, and D. Robinson

***Abstract*—Voltage fluctuations leading to lamp flicker that originate in one place in a power system tend to propagate to other parts of the network with some level of attenuation depending on the network impedances and the loads connected. Numerous subsynchronous-type frequency components exist in these voltage fluctuations that are responsible for lamp flicker. The rudimentary theory and the experimental measurements support the idea that industrial load bases, which contain a large percentage of mains-connected induction motors, tend to attenuate flicker better compared to residential load bases having mainly passive loads. This paper reports on the response of three-phase induction motors of several sizes when subjected to low-frequency voltage fluctuations: 1) the case where a balanced single-frequency component is superimposed on the mains voltage and 2) the case where the mains voltage is sinusoidally amplitude modulated, a scheme that is frequently used in the flicker-related work. Small-signal models are presented that will enable systematic understanding of the behavior which is verified using large signal models.**

***Index Terms*—Flicker, flicker attenuation, induction motors, small-signal models.**

I. Introduction

THE rudimentary theory behind flicker propagation, the importance of flicker transfer coefficient, and supporting measurement results are documented in a few papers [1]–[6]. These suggest that the attenuation of flicker is dependent on a few factors, including the composition of loads at the various busbars. It is suggested that mains-connected induction motors tend to help attenuate flicker better compared to passive loads.

The argument behind flicker attenuation provided by induction motors is illustrated through the simple radial system shown in Fig. 1. Upstream (A) to downstream (B) flicker transfer coefficient [7], [8] is considered to be equal to the ratio of the relative voltage changes as given by [1]

$$T_{PstAB} = \frac{\left|\frac{\Delta v_B}{v_B}\right|}{\left|\frac{\Delta v_A}{v_A}\right|} = \frac{\left|1+\frac{Z_S}{Z_L}\right|}{\left|1+\frac{Z'_S}{Z'_L}\right|} \quad (1)$$

where

v_A, v_B	magnitude of the steady state voltages at A and B, respectively;
Δv_A, Δv_B	fluctuations in the magnitudes of the voltages at A and B, respectively;

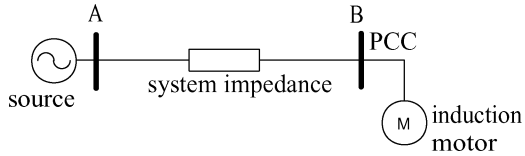

Fig. 1. Simple radial system.

Z_L	steady-sate impedance of the motor;
Z'_L	effective impedance of the motor for small voltage fluctuations;
Z_S	impedance of the system that connects the upstream and the downstream (e.g., transformer impedance);
Z'_S	effective Z_S for small voltage fluctuations.

It is hypothesizd that the effective impedance of the induction motor load under fluctuating conditions is less than its steady-state impedance (i.e., $|Z'_L| < |Z_L|$) and assuming $|Z_S| = |Z'_S|$, it is seen from (1) that $T_{PstAB} < 1.0$.

Despite the aforementioned hypothesis, the available literature on the subject of flicker transfer does not cover any details on the manner in which the induction motors respond to voltage fluctuations. Some theory in relation to the three-phase induction motor behavior, where they are tested by superimposing a second frequency component, is covered in several papers [9], [10], yet a detailed understanding of the way stator current responds in relation to the operating situation is not the subject as expected. Further, the dependency of this response on the frequency of voltage fluctuations is also not known.

The main objective of the work covered in this paper is to examine the dynamic behavior of three-phase induction motors to regular fluctuations in the terminal voltage. This paper presents the results obtained using large-signal and small-signal models in relation to three-phase induction motor behavior for 1) where a single-frequency component is superimposed and 2) where the mains voltage is sinusoidally amplitude modulated, a classical case considered in flicker studies. The models presented and the results obtained in the paper can be subsequently used to further investigate the manner in which induction machines help attenuate flicker.

This paper is organized as follows. The background details in relation to modelling presented in the paper are given in Section II. The analysis of induction machine stator current response to fluctuating voltage supply, where fluctuations are caused by a single-frequency component, is presented in Section III. The stator current response to a sinusoidally amplitude-modulated fluctuating supply, using both large-signal and small-signal analysis, is presented in Section V. Conclusions are given in Section VI.

Manuscript received January 5, 2007; revised March 27, 2007. This work was supported by TransGrid. Paper no. TPWRD-00828-2006.

S. Tennakoon and S. Perera are with the School of Electrical, Computer, and Telecommunications Engineering, University of Wollongong, and are with the Integral Energy Power Quality and Reliability Centre, Wollongong NSW 2522, Australia (e-mail: sarath@uow.edu.au).

D. Robinson is with Beca Pty. Ltd., Wollongong NSW 2500, Australia.

Digital Object Identifier 10.1109/TPWRD.2007.908788

II. Background Details on the Study of Large-Signal and Small-Signal Modelling of Induction Motors

In order to gain a broader understanding, four different machines with ratings ranging from 3- to 2250-hp 60-Hz motors of which the parameters given in [11] are considered in this work. A conventional dq-domain large-signal model simulated in Matlab/Simulink and small-signal models covered in Appendices A and B are used to analyze the behavior of the induction motors.

The mechanical load driven by the motors is assumed to be that of pump type with per-unit torque-speed characteristics given by

$$(T_L)_{\rm pu} = k\left(\frac{\omega_r}{\omega_b}\right)^2 \tag{2}$$

where T_L is the load torque, ω_r is the rotor angular speed of the motor, ω_b is the base angular speed, and k is a constant.

III. Stator Current Response to Voltage Fluctuations Caused by a Superimposed Positive-Sequence Component

Frequency f_i of the superimposed positive sequence voltage can be greater or smaller than the mains frequency f_b. For this reason and also because the resulting stator current exhibits frequency components that are additional to what is caused by f_b and f_i individually, it is necessary to establish a means of identifying the various voltage and current components. In the present situation, the frequency components of currents that appear have a strong resemblance to sinusoidal amplitude modulation where the mains frequency voltage waveform is amplitude modulated at f_m, which leads to two sideband frequency components $f_b - f_m$ and $f_b + f_m$. Thus, any single-frequency component f_i superimposed that has a frequency

- less than f_b will be called lower sideband injection with a voltage $\Delta v_{\rm LSB}$, satisfying the relationship $f_i = f_b - f_m$, where 40 Hz$\leq$ f_m $\leq$0.01 Hz leading to 20 Hz$\leq$ f_i $\leq$ 59.99 Hz.
- greater than f_b will be called upper sideband injection with a voltage $\Delta v_{\rm USB}$ satisfying the relationship $f_i = f_b + f_m$, where 0.01 Hz$\leq$ f_m $\leq$ 40 Hz leading to 60.0 Hz$\leq$ f_i $\leq$ 100 Hz.

Further, relating to the case of sinusoidal amplitude modulation, each side band will have a peak value of $V_m/2$, where V_m is the peak value of the modulating wave.

Assuming the peak value of the mains voltage to be given by V_p, the three line-to-neutral voltages for positive-sequence injection are given by

$$v_{a,b,c} = V_p \sin\left(\omega_b t - (n-1)\frac{2\pi}{3}\right) + \frac{V_m}{2}\sin\left(\omega_i t - (n-1)\frac{2\pi}{3}\right) \tag{3}$$

where $\omega_b = 2\pi f_b$, $\omega_i = 2\pi f_i$, and $n = 1,2,3$.

Due to the presence of two airgap magnetic fields—one due to the mains voltage and the other due to the superimposed voltage, both of the same phase sequence—the electromagnetic torque of the motor will pulsate at a difference frequency $|f_b - f_i|$, leading to a pulsation in the mechanical speed at the same difference frequency, a behavior commonly referenced in relation to inverter-driven induction motors. Small-signal analysis covering the determination of this speed fluctuation is given in Appendix C.

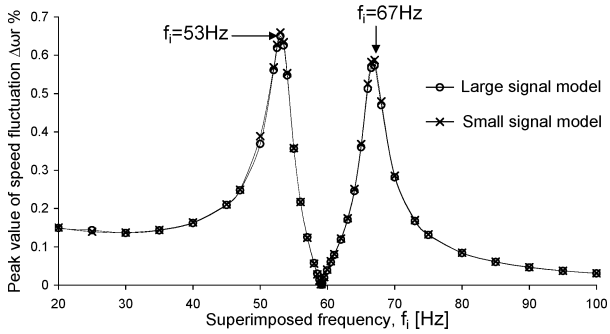

Fig. 2. Rotor speed fluctuation of the 2250-hp motor with injected frequency established using small- and large-signal analyses.

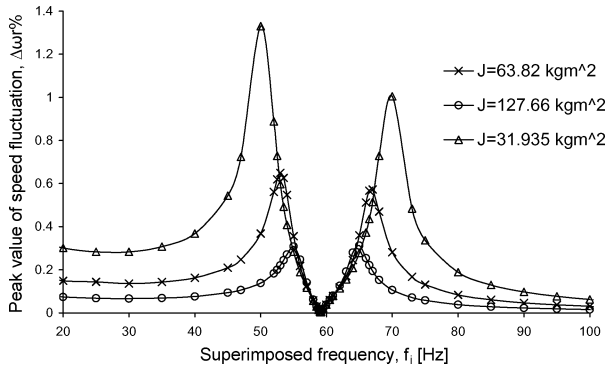

Fig. 3. Comparison of rotor speed fluctuation of the 2250-hp motor for three different inertia values.

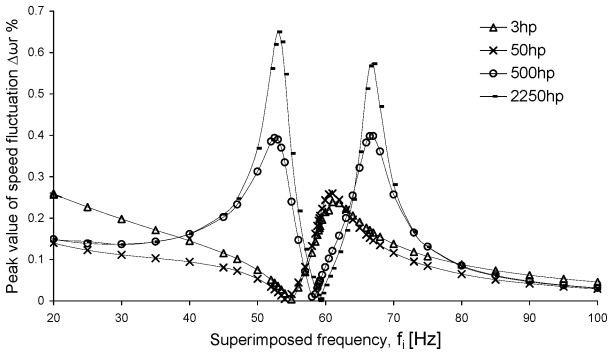

Fig. 4. Comparison of rotor speed fluctuation of different motors with injected frequency.

In the large-signal simulations carried out, the amplitude of the superimposed voltage was maintained constant such that $V_m/2 = 0.025$ V$_p$.

Fig. 2 shows the variation of the peak value of the speed fluctuation $(\Delta\omega_r)$ as a percentage of the steady-state speed for the 2250-hp motor with the nominal value of inertia given in [11]. Fig. 3 shows the results from large-signal analysis illustrating how the speed fluctuations are affected by the inertia. Fig. 4 illustrates the results from large-signal analysis comparing the speed fluctuation exhibited by the four different machines. Although the amplitude of speed fluctuation is relatively small, it

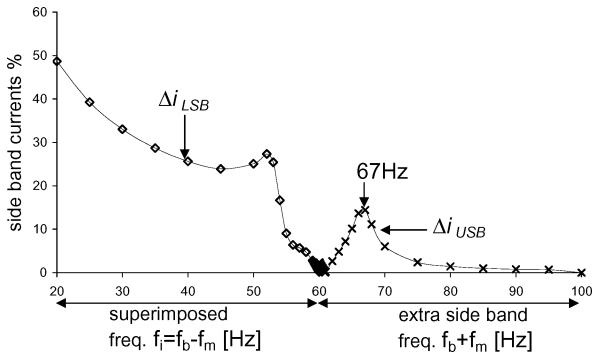

Fig. 5. Variation of stator current sidebands for lower sideband injection, 2250-hp motor $f_i = f_b - f_m$.

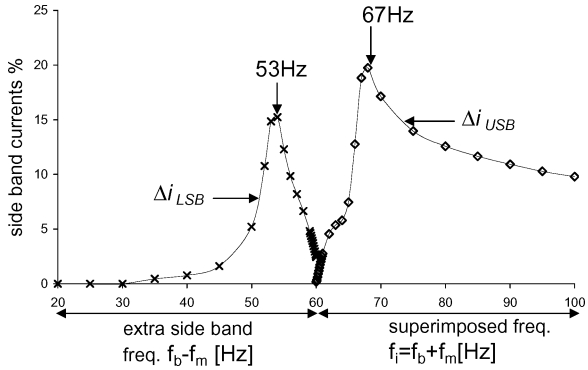

Fig. 6. Variation of stator current sidebands for upper sideband injection, 2250-hp motor $f_i = f_b + f_m$.

has a strong influence on the stator current over the frequency range of interest in relation to flicker. The manner in which the resulting stator current interacts with the rotor thus affecting the level of speed oscillation can be explained in terms of negative and positive damping as in the case of subsynchronous resonance in power systems. Appendix D gives a qualitative discussion on this self-perpetuating behavior, employing the results that are presented in this section.

Using the simple theory behind stator frequency components and its interaction with the rotor, which is now oscillating at a difference frequency of $|f_b - f_i| = f_m$, it is possible to establish the frequencies that are induced back in the stator. As such, if the superimposed frequency component is a lower sideband (i.e., $f_i = f_b - f_m$), extra frequency components will be induced in the stator at $f_b + f_m$ and $f_b \pm 2jf_m$, where j is integer (1, 2, 3, etc.). However, through the time-domain simulations carried out, it has been noted that among the corresponding extra sideband currents, $f_b + f_m$ is the most significant component while $f_b \pm 2jf_m$ components have relatively negligible magnitudes for all superimposed frequencies and, hence, are ignored. Similar analysis can be carried out when the superimposed frequency is an upper sideband (i.e., $f_i = f_b + f_m$), where the extra frequency components will be induced at $f_b - f_m$ of the most significant magnitude, and $f_b \pm 2jf_m$ with negligible magnitudes enabling them to be ignored. Hence, the only extra sidebands considered for lower and upper sideband injection of this work are those appearing at $f_b + f_m$ and $f_b - f_m$, respectively.

Fig. 5 shows the variation of the magnitudes of the two sideband components (Δi_{LSB} and Δi_{USB}) of stator current for the 2250-hp machine for lower sideband injection. In addition to the superimposed current component at $f_i = f_b - f_m$, an extra upper sideband component of stator current at a frequency at $(f_b + f_m)$ can be noted here. The magnitudes of the sideband currents, to varying levels, are influenced by both 1) level of speed fluctuation which governs the corresponding induced voltage and 2) frequency of the sideband current which influences the effective impedance for current flow. With reference to Fig. 2, at an injected frequency of 53 Hz, the speed fluctuation exhibits a local maximum. The corresponding upper sideband frequency is therefore 67 Hz which lines up with the peak value of the upper sideband current in Fig. 5. As the injected frequency is further decreased below 53 Hz, the magnitude of speed fluctuations decreases and the frequency of the upper sideband frequency increases and, hence, the extra sideband current is seen to reduce. The current caused by the injected frequency f_i is seen to generally increase as its frequency is decreased which suggests that this variation is relatively significantly affected by the frequency rather than the speed fluctuation that is now relatively low.

Fig. 6 shows the variation of the magnitudes of the two sideband components (Δi_{LSB} and Δi_{USB}) of stator current for the 2250-hp machine for upper sideband injection ($f_i = f_b + f_m$). The extra sideband can be seen at $f_b - f_m$. Referring to Fig. 2, the speed fluctuation exhibits a local maxima at 67 Hz which corresponds to an extra lower sideband at 53 Hz, exhibiting a local maximum as seen in Fig. 6. As the injected frequency is further increased, the speed fluctuations decrease and, hence, the resulting lower sideband current is seen to decrease. The current caused by the injected frequency is seen to exhibit a significant local maximum at 67 Hz. It appears that this component of current is affected significantly by the speed fluctuation as well as frequency. Beyond 67 Hz, the current becomes increasingly governed by the increasing frequency of the injected voltage. Simulations quite clearly illustrate that the superposition principle commonly used for the analysis of induction motors subjected to mains frequencies carrying superimposed frequencies becomes increasingly valid only at higher superimposed frequencies.

Comparing Figs. 5 and 6, it can be noted that the total fluctuating current component (combination of the currents due to injected frequency and the extra sideband) is seen to be relatively large when the injected frequency is low (i.e., 20 Hz) when compared with that at the high frequency end (i.e., 100 Hz). Based on the above behavior, as a preliminary observation, it can be stated that the rms voltage fluctuations arising as a result of the motor behavior are very much dependent on the frequency of the voltage fluctuations.

Figs. 7 and 8 illustrate the variation of sideband currents for lower and upper sideband injection, respectively, for the four different machines. It is clear from these figures that the two large machines behave differently than the two small machines. For lower sideband injection, the large machines exhibit significant lower and upper sideband currents over a wide frequency range, while the two small machines exhibit significant lower sideband currents and not upper sideband currents. For upper sideband injection, the two large machines exhibit significant upper and lower sideband currents while the two small machines exhibit significant upper sideband currents while the lower sideband currents are seen to be relatively small.

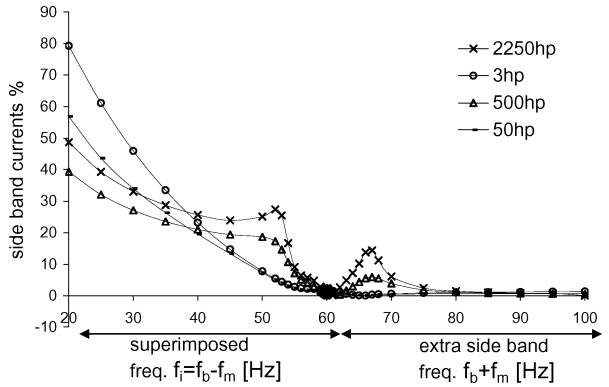

Fig. 7. Comparison of stator current sidebands of different motors for lower sideband injection.

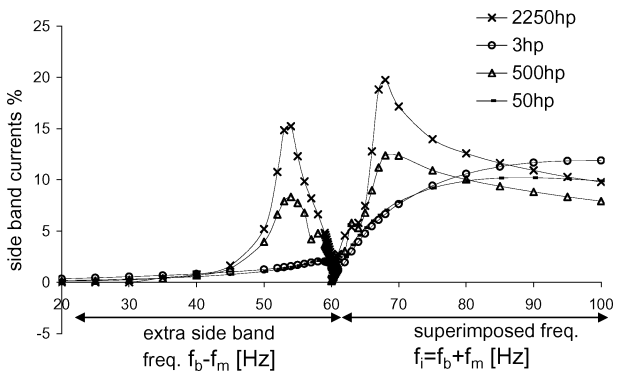

Fig. 8. Comparison of stator current sidebands of different motors for upper sideband injection.

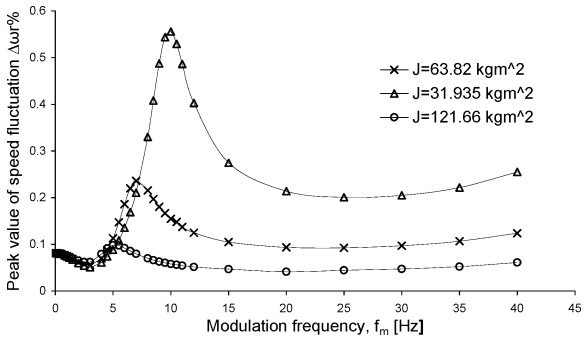

Fig. 9. Rotor speed fluctuation of the 2250-hp motor for AM.

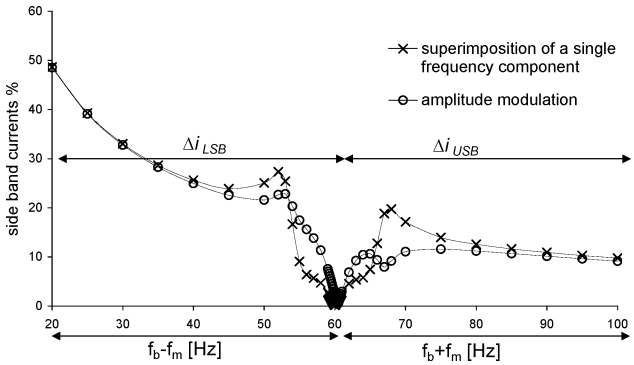

Fig. 10. Variation of stator sideband current components (as a percentage of the fundamental) with sideband frequency ($f_b - f_m$ or $f_b + f_m$) established for amplitude modulation and superimposition of a single-frequency component.

IV. Stator Current Response to Voltage Fluctuations Caused by a Superimposed Negative-Sequence Component

With negative-sequence injection rotor speed, fluctuation will take place at $f_b + f_i$. Simulations reveal that the corresponding level of speed fluctuation is relatively insignificant compared to that corresponding to positive-sequence injection. The resulting additional components of current induced in the stator are at higher frequencies that are outside the normal flicker frequency range of interest. Also, these high-frequency current components are of negligible magnitude and, hence, would be of little relevance in relation to voltage fluctuations and flicker.

V. Stator Current Response to Voltage Fluctuations Caused by Sinusoidal Amplitude Modulation

A. Large Signal Behavior

Assuming balanced sinusoidal amplitude modulation, the line-to-neutral voltages applied to a three-phase motor can be defined as

$$v_{a,b,c} = V_p\left[1 + m\sin(2\pi f_m t)\right]\cos\left(2\pi f_b t - (n-1)\frac{2\pi}{3}\right) \tag{4}$$

where $n = 1,2,3$ and $m = V_m/V_p$—modulation depth

In the simulations carried out, the modulating waveform was selected such that $V_m = 0.05\mathrm{V}_p$ so that each sideband voltage arising as a result is equal to the superimposed component in the case of single-frequency injection. As in the case of single-frequency injection, the machines exhibited speed fluctuations at f_m. For the 2250-hp machine, these speed fluctuations are illustrated in Fig. 9, demonstrating their dependency of inertia as well.

As expected, stator current exhibits component currents at $f_b - f_m$ and $f_b + f_m$ although of different magnitudes as illustrated by Fig. 10. Relatively negligible sideband currents at frequencies of $f_b \pm 2jf_m$ were noticed which will be neglected in further analytical work. Fig. 10 also shows the magnitudes of the current corresponding to the injected frequency obtained in relation to single-frequency injection (shown in Figs. 5 and 6). The differences in the current levels clearly indicate that in the case of amplitude modulation, the resulting sideband current is due to the net effect of multiple armature reaction and they cannot be obtained by simply considering that due to the single-frequency injection. For example, the sideband current magnitude corresponding to a frequency of 40 Hz (which is caused by a modulating frequency of $f_m = 20$ Hz) is caused by the armature reaction due to a current sideband at a frequency of 80 Hz as well.

B. Small-Signal Analysis

In contrast to single-frequency injection where an additional component is superimposed on the mains voltage, in sinusoidal amplitude modulation (AM), it is the amplitude of the mains voltage which is fluctuating sinusoidally. Thus, a transfer function of the form

$$G(s) = \frac{\Delta i_s}{\Delta v_s} \tag{5}$$

where $\Delta v_s =$ small signal change in the amplitude of the supply voltage and $\Delta i_s =$ small signal change in the stator current, can be developed to examine how the induction motors respond to voltage perturbations caused by AM.

For a balanced set of sinusoidal supply voltages, the dq axes voltages are of the form

$$\begin{bmatrix} v_{\rm qs} \\ v_{\rm ds} \end{bmatrix} = \begin{bmatrix} V_p \\ 0 \end{bmatrix}. \tag{6}$$

Thus, for a small perturbation (Δv_s) in the supply-voltage magnitude

$$\begin{bmatrix} \Delta v_{\rm qs} \\ \Delta v_{\rm ds} \end{bmatrix} = \begin{bmatrix} \Delta v_s \\ 0 \end{bmatrix} \tag{7}$$

Δv_s is defined as a sinusoidal signal per (8) in order to represent a typical modulating signal at a frequency f_m.

$$\Delta v_s = \frac{V_m}{V_p} \sin \omega_m t. \tag{8}$$

The small-signal stator currents are related to the state vector per (9)

$$y = Cx \tag{9}$$

where

$$y = [\Delta i_{\rm qs} \quad \Delta i_{\rm ds}]^T \tag{10}$$

$$C = \frac{1}{D} \begin{bmatrix} X'_{rr} & 0 & -X_M & 0 & 0 \\ 0 & X'_{rr} & 0 & -X_M & 0 \end{bmatrix}. \tag{11}$$

Modifying the control vector (B.16) in Appendix B to incorporate stator voltage perturbations given by (7) and solving state space equations (B.14) and (9), two fifth-order transfer functions ($G_1(s)$ and $G_2(s)$) can be established as

$$\begin{bmatrix} \frac{\Delta i_{\rm qs}}{\Delta v_s} \\ \frac{\Delta i_{\rm ds}}{\Delta v_s} \end{bmatrix} = \begin{bmatrix} G_1(s) \\ G_2(s) \end{bmatrix} \tag{12}$$

where $\Delta i_{\rm qs}$ and $\Delta i_{\rm ds}$ need to be transformed to the phase domain to establish the stator current variations as a function of the perturbation in the supply voltage. These perturbations will yield the sidebands of the stator current $\Delta i_{\rm LSB}$ and $\Delta i_{\rm USB}$ when Fourier is analyzed. The aforementioned process is illustrated by the block diagram of Fig. 11.

The comparison of sideband current magnitudes obtained by employing small-signal analysis and those obtained from large-signal analysis, illustrated in Fig. 12, clearly demonstrate the suitability of the small-signal models for the prediction of the perturbations in the stator current.

Fig. 13 shows the stator current responses of the four different machines considered. As in the case of single-frequency injection, the four machines can be categorized into two groups based on the stator response since the large machines (2250 and 500 hp) and the small machines (50 and 3 hp) exhibit distinctly different behaviors. This suggests that depending on the machine size and their parameters, different induction machines can lead to different flicker attenuation characteristics.

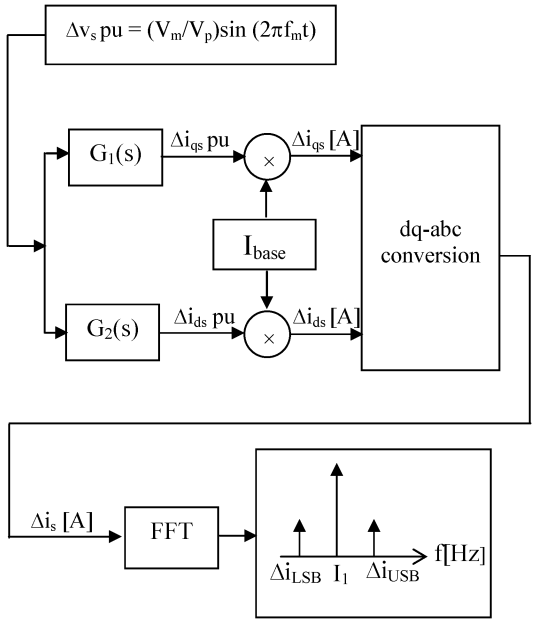

Fig. 11. Recovery of stator current perturbation (Δi_s).

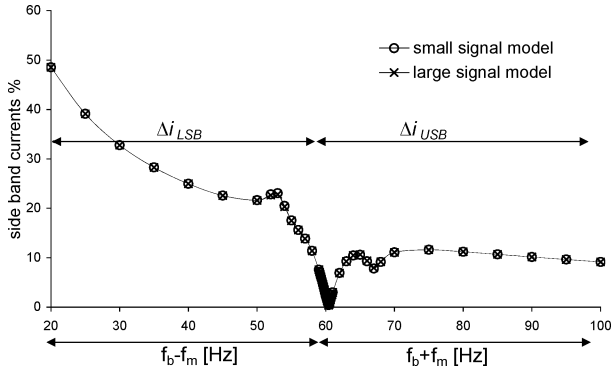

Fig. 12. Variation of stator sideband current components (as a percentage of the fundamental) established using small- and large-signal analyses for amplitude modulation.

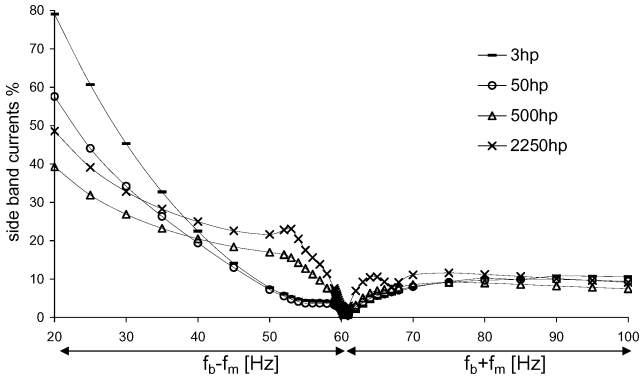

Fig. 13. Comparison of the sideband currents caused by amplitude modulation for motors of different sizes.

VI. Conclusion

The response of induction motors to regular voltage fluctuations in the flicker frequency range has been investigated using both large- and small-signal models. It is evident that the speed

fluctuation that takes place can lead to extra frequency components of significance. These extra components appear as sidebands in relation to the mains frequency and the superimposed low-frequency component in the case of single-frequency injection of which the major ones have been identified. In the case of sinusoidal amplitude modulation, the major sidebands in the current are related to the mains frequency and the sinusoidal modulating frequency. Again, the main components of significance have been identified. In both cases, these sideband currents have been noted to be dependent on the injection frequency or the modulating frequency thus indicating the dependency of flicker attenuation on the frequency of fluctuations. The models developed in this paper can be extended to examine the flicker attenuation in power transmission and distribution systems where some approximate load classification can be carried to account for the induction motor population.

APPENDIX A
NOMENCLATURE

v_d, v_q	dq axes voltages (in volts).
v'_d, v'_q	dq axes voltages referred to stator (in volts).
ψ_d, ψ_q	dq axes flux linkages per second (in volts).
ψ'_d, ψ'_q	dq axes flux linkages per second referred to the stator (in volts).
r_s	Stator resistance (in ohms).
X_{ls}	Stator leakage reactance (in ohms).
r'_r	Rotor resistance (referred to the stator) (in ohms).
X'_{lr}	Stator leakage reactance (referred to the stator) (in ohms).
X_M	Mutual reactance (in ohms).
J	Moment of inertia.
H	Inertia constant.
ω_b	Base angular frequency (in radians per second).
ω_e	Synchronous speed (in radians per second).
ω_r	Rotor angular speed (electrical) (in radians per second).
p	d/dt operator.
s	Laplace operator.

Subscripts

s	Stator variables.
r	Rotor variables.
o	Steady-state values.

APPENDIX B
LINEARIZED MOTOR EQUATIONS

For balanced operation of a three-phase induction motor, the voltage equations in the synchronously rotating reference frame are given by (B.1) [11], as shown in the equation at the bottom of the page, where

$$X_{ss} = X_{ls} + X_M \tag{B.2}$$
$$X'_{rr} = X'_{lr} + X_M \tag{B.3}$$
$$D = X_{ss}X'_{rr} - X_M^2. \tag{B.4}$$

The machine variables in (B.1) are expressed as per-unit quantities using the following base values:

V_{base}	line-to-neutral peak voltage (V_p);
I_{base}	peak line current (I_p).

The electromagnetic torque (T_e) and its relationship with the rotor angular speed (ω_r) are given by (B.5) and (B.6)

$$T_e = \frac{X_M}{D}\left(\psi'_{dr}\psi_{\text{qs}} - \psi'_{\text{qr}}\psi_{\text{ds}}\right) \tag{B.5}$$
$$T_e = 2Hp\frac{\omega_r}{\omega_b} + T_L. \tag{B.6}$$

Equations (B.1), (B.5), and (B.6) can be linearized around an operating point to examine the small-signal behavior of the motor. These linearized voltage equations are given by (B.7), as shown in the equation at the bottom of the page, where

$$\omega_e = \omega_b \tag{B.8}$$
$$s_o = \frac{\omega_e - \omega_{ro}}{\omega_e} \tag{B.9}$$

$$\begin{bmatrix} v_{\text{qs}} \\ v_{\text{ds}} \\ v'_{\text{qr}} \\ v'_{dr} \end{bmatrix} = \begin{bmatrix} \frac{r_s X'_{rr}}{D} + \frac{p}{\omega_b} & \frac{\omega_e}{\omega_b} & -\frac{r_s X_M}{D} & 0 \\ -\frac{\omega_e}{\omega_b} & \frac{r_s X'_{rr}}{D} + \frac{p}{\omega_b} & 0 & -\frac{r_s X_M}{D} \\ -\frac{r_r X'_M}{D} & 0 & \frac{r'_r X_{ss}}{D} + \frac{p}{\omega_b} & \frac{\omega_e - \omega_r}{\omega_b} \\ 0 & -\frac{r'_r X_M}{D} & -\frac{\omega_e - \omega_r}{\omega_b} & \frac{r'_r X_{ss}}{D} + \frac{p}{\omega_b} \end{bmatrix} \begin{bmatrix} \psi_{\text{qs}} \\ \psi_{\text{ds}} \\ \psi'_{\text{qr}} \\ \psi'_{dr} \end{bmatrix} \tag{B.1}$$

$$\begin{bmatrix} \Delta v_{\text{qs}} \\ \Delta v_{\text{ds}} \\ \Delta v'_{\text{qr}} \\ \Delta v'_{dr} \end{bmatrix} = \begin{bmatrix} \frac{r_s X'_{rr}}{D} + \frac{p}{\omega_b} & \frac{\omega_e}{\omega_b} & -\frac{r_s X_M}{D} & 0 & 0 \\ -\frac{\omega_e}{\omega_b} & \frac{r_s X'_{rr}}{D} + \frac{p}{\omega_b} & 0 & -\frac{r_s X_M}{D} & 0 \\ -\frac{r'_r X_M}{D} & 0 & \frac{r'_r X_{ss}}{D} + \frac{p}{\omega_b} & \frac{\omega_e - \omega_{ro}}{\omega_b} & \psi'_{\text{dro}} \\ 0 & -\frac{r'_r X_M}{D} & -\frac{\omega_e - \omega_{ro}}{\omega_b} & \frac{r'_r X_{ss}}{D} + \frac{p}{\omega_b} & \psi'_{\text{dro}} \end{bmatrix} \begin{bmatrix} \Delta\psi_{\text{qs}} \\ \Delta\psi_{\text{ds}} \\ \Delta\psi'_{\text{qr}} \\ \Delta\psi'_{dr} \\ \frac{\Delta\omega_r}{\omega_b} \end{bmatrix} \tag{B.7}$$

Using (B.5) and (B.6), the electromagnetic torque is obtained as follows:

$$T_L = \frac{X_M}{D}\left(\psi'_{dr}\psi_{\rm qs} - \psi'_{\rm qr}\psi_{\rm ds}\right) - 2Hp\frac{\omega_r}{\omega_b}. \tag{B.10}$$

Linearizing (B.10)

$$\Delta T_L = \frac{X_M}{D}\left(\psi'_{\rm dro}\Delta\psi_{\rm qs} - \psi'_{\rm qro}\Delta\psi_{\rm ds} - \psi_{\rm dso}\Delta\psi'_{\rm qr} + \psi_{\rm qso}\Delta\psi'_{dr}\right) - 2Hp\frac{\Delta\omega_r}{\omega_b}. \tag{B.11}$$

If the load torque-speed characteristics are known, (B.11) can be further modified. Here, a pump load with characteristics given by (2) is assumed. Linearizing (2)

$$\Delta T_L = \left(\frac{2k\omega_{ro}}{\omega_b}\right)\frac{\Delta\omega_r}{\omega_b}. \tag{B.12}$$

Using (B.11) and (B.12), the dynamics of the motor and the pump load can be combined as

$$\frac{X_M}{D}\left(\psi'_{\rm dro}\Delta\psi_{\rm qs} - \psi'_{\rm qro}\Delta\psi_{\rm ds} - \psi_{\rm dso}\Delta\psi'_{\rm qr} + \psi_{\rm qso}\Delta\psi'_{dr}\right) - \left(2Hp\frac{\Delta\omega_r}{\omega_b} + \frac{2k\omega_{ro}}{\omega_b}\frac{\Delta\omega_r}{\omega_b}\right) = 0. \tag{B.13}$$

Linearized voltage equations and the torque-speed dynamic relationship given by (B.7) and (B.13), respectively, describe the small-signal model of an induction motor that drives a pump load and can be expressed in state space form as given by (B.14)

$$px = Ax + Bu \tag{B.14}$$

where

$$x = \left[\Delta\psi_{\rm qs}\ \Delta\psi_{\rm ds}\ \Delta\psi'_{\rm qr}\ \Delta\psi'_{dr}\ \frac{\Delta\omega_r}{\omega_b}\right]^T \tag{B.15}$$

$$u = \left[\Delta v_{\rm qs}\ \Delta v_{\rm ds}\ \Delta v'_{\rm qr}\ \Delta v'_{dr}\right]^T \tag{B.16}$$

in which $\Delta v'_{\rm qr}$ and $\Delta v'_{dr}$ are both equal to zero and the matrices $[A]$ and $[B]$ can be established as

$$A = \begin{bmatrix} -\frac{r_s X'_{rr}}{D} & -1 & \frac{r_s X_M}{D} & 0 & 0 \\ 1 & -\frac{r_s X'_{rr}}{D} & 0 & \frac{r_s X_M}{D} & 0 \\ \frac{r'_r X_M}{D} & 0 & -\frac{r_r X_{ss}}{D} & -s_o & \psi'_{\rm dro} \\ 0 & \frac{r'_r X_M}{D} & s_o & -\frac{r'_r X_{ss}}{D} & -\psi'_{\rm qro} \\ \frac{X_M\psi'_{\rm dro}}{2HD\omega_b} & -\frac{X_M\psi'_{\rm qro}}{2HD\omega_b} & -\frac{X_M\psi_{\rm dso}}{2HD\omega_b} & \frac{X_M\psi_{\rm qso}}{2HD\omega_b} & -\frac{k\omega_{ro}}{2H\omega_b^2} \end{bmatrix} \tag{B.17}$$

$$B = \omega_b \begin{bmatrix} 1 & 0 & 0 & 0 \\ 0 & 1 & 0 & 0 \\ 0 & 0 & 1 & 0 \\ 0 & 0 & 0 & 1 \\ 0 & 0 & 0 & 0 \end{bmatrix}. \tag{B.18}$$

APPENDIX C
SMALL-SIGNAL ANALYSIS OF SPEED FLUCTUATIONS

For a supply voltage consisting of a superimposed positive-sequence sinusoidal single-frequency component, the three-phase voltages given by (3) can be transformed into a dq frame to obtain $\Delta v_{\rm qs}$ and $\Delta v_{\rm ds}$. These small-signal excursions expressed as per-unit quantities are given by

$$\Delta v_{\rm qs} = \frac{V_m}{2V_p}\cos\omega_m t \tag{C.1}$$

$$\Delta v_{\rm ds} = -\frac{V_m}{2V_p}\sin\omega_m t. \tag{C.2}$$

Using (B.14) in B, the state vector that contains rotor speed fluctuation can be established as

$$x = (sI - A)^{-1}u. \tag{C.3}$$

Using the matrix A and vector u, the steady-state fluctuation in the speed as a normalized quantity can be shown to take the form as given by (C.4)

$$\frac{\Delta\omega_r}{\omega_b} = m_1\cos\omega_m t + m_2\sin\omega_m t \tag{C.4}$$

where m_1 and m_2 are constants, thus confirming the speed fluctuation at ω_m.

APPENDIX D
DISCUSSION ON THE POSITIVE AND NEGATIVE DAMPING PROVIDED BY THE STATOR SIDEBAND CURRENTS

A qualitative discussion on the manner in which the magnitude of the speed fluctuation varies over the range of superimposed frequencies can be developed using Fig. 2 in conjunction with Figs. 5 and 6. In relation to the two latter figures, a stator current component at $f_b - f_m$ will provide negative damping and that at $f_b + f_m$ will provide positive damping to the speed oscillations and, at all times, the magnitude of the speed oscillations will be curtailed by the net damping available. With reference to a particular injected frequency, the corresponding magnitude of the stator sideband current will be governed by the effective impedance whereas the magnitude of the extra sideband current will be governed by both the effective impedance and the level-induced voltage which is determined by the magnitude of the speed oscillations. Thus, the speed oscillations and the stator currents, especially the extra sideband current, can be said to be interdependent.

Considering the case of lower sideband injection, at injected frequencies close to 60 Hz, the frequency and the magnitude of speed oscillation and the corresponding lower and upper sideband stator currents are relatively small. As the injected frequency is reduced below 60 Hz, the corresponding current will increase which is a process essentially governed by the decreasing effective impedance. This current leads to an increasing upper sideband-induced voltage resulting in increasing upper sideband current. Increasing negative damping provided by the lower sideband and increasing positive damping provided by the upper sideband would lead to speed oscillations with a local maxima at 53 Hz as evident from Fig. 2. As the injected

frequency is further reduced below 53 Hz, the lower sideband current continues to increase as a result of the decreasing effective impedance whereas the upper sideband current starts to decrease above 67 Hz as a result of increasing frequency and reducing induced voltage. Despite the decreasing positive damping provided by the upper sideband current in this frequency range (67 Hz–100 Hz), the speed oscillations continue to exist well below 53 Hz, implying that the increasing negative damping provided by the lower sideband current dominates the net damping.

Considering the case of upper sideband injection, at close to 60 Hz, the upper sideband current is seen to increase as a result of the dominating but decreasing positive effective rotor resistance. The corresponding lower sideband current magnitude will be governed by the effective impedance at lower frequencies and will continue to provide negative damping. It is seen that the net damping provides a local maxima at an injected frequency of 67 Hz. As the injected frequency is further increased beyond 67 Hz, both the positive and negative damping are seen to decrease, causing the speed oscillations to decrease. It is seen that the lower sideband current approaches negligible levels as the speed oscillations diminish.

REFERENCES

[1] E. De Jaeger, G. Borloo, and W. Vancoetsem, "Flicker transfer coefficients from HV to MV and LV systems," in *Proc. 14th Int. Conf. Electricity Distribution, Session 2*, Birmingham, U.K., Jun. 1997, pp. 101–102.

[2] H. Renner and M. Sakulin, "Flicker propagation in meshed high voltage networks," in *Proc. 9th Int. Conf. Harmonics Quality Power*, Oct. 2000, vol. 3, pp. 1023–1028.

[3] S. M. K. Tennakoon, L. Perera, D. Robinson, and S. Perera, "Flicker transfer in radial power systems," presented at the Australasian Universities Power Eng. Conf., Brisbane, Australia, Sep. 2004, Paper 190, unpublished.

[4] M. C. Simöes and S. M. Deckmann, "Flicker propagation and attenuation," in *Proc. 10th Int. Conf. Harmonics Quality Power*, Oct. 2002, vol. 2, pp. 644–648.

[5] S. Perera, D. Robinson, S. Elphick, D. Geddey, N. Browne, V. Smith, and V. Gosbell, "Synchronised flicker measurement for flicker transfer evaluation in power systems," *IEEE Trans. Power Del.*, vol. 21, no. 3, pp. 1477–1482, Jul. 2006.

[6] S. Tennakoon, S. Perera, D. Robinson, and S. Elphick, "Attenuation of flicker by induction motors: A laboratory investigation," presented at the 12th Int. Conf. Harmonics Quality of Power, Cascais, Portugal, Oct. 2006, Paper 88, unpublished.

[7] *Electromagnetic Compatibility (EMC)—Part 3: Limits—Section 7: Assessment of Emission Limits for Fluctuating Loads in MV and HV Power Systems*, IEC/TR 61000-3-7, Ed. 1.0, 1996.

[8] *Electromagnetic Compatibility (EMC)—Limits—Assessment of Emission Limits for Fluctuating Loads in MV and HV Power Systems (IEC 61000-3-7:1996, MOD)*, AS/NZS 61000.3.7:2001, Standards Australia.

[9] H. R. Schwenk, "Equivalent loading of induction machines for temperature tests," *IEEE Trans. Power App. Syst.*, vol. PAS-96, no. 4, pp. 1126–1131, Jul./Aug. 1977.

[10] C. Grantham, H. Tabatabaei-Yazdi, and M. F. Rahman, "Efficiency evaluation of three phase induction motors by synthetic loading," in *Proc. Int. Conf. Power Electronics Drive Systems*, May 1997, vol. 1, pp. 103–109.

[11] P. C. Krause, O. Wasynczuk, and S. D. Sudhoff, *Analysis of Electric Machinery*, 2nd ed. New York: Wiley, 2002.

[12] J. P. G. de Abreu and A. E. Emanuel, "The need to limit subharmonics injection," in *Proc. 9th Int. Conf. Harmonics Quality of Power*, Oct. 2000, vol. 1, pp. 251–253.

S. Tennakoon (S'06) received the B.Eng. (Hons.) degree in electrical power engineering from the University of Moratuwa, Sri Lanka, and is currently pursuing the Ph.D. degree at the University of Wollongong, Wollongong, Australia.

She is a recipient of an International Postgraduate Research Scholarship (IPRS) from the University of Wollongong. Her research interests are in power quality and electrical machine modelling.

S. Perera (M'95) received the B.Eng. degree in electrical power engineering from the University of Moratuwa, Sri Lanka, the M.Eng. degree from the University of New South Wales, Sydney, Australia, and the Ph.D. degree from the University of Wollongong, Wollongong, Australia.

He has been a lecturer at the University of Moratuwa. Currently he is an Associate Professor with the University of Wollongong, where he is also the Technical Director of the Integral Energy Power Quality and Reliability Centre.

D. Robinson received the B.E. (Hons.) and Ph.D. degrees in harmonics management from the University of Wollongong, Wollongong, Australia.

He was with BHP Steel, Port Kembla, Australia, and the University of Wollongong. Currently, he is with Beca Pty. Ltd., Wollongong.